Preprint: IEEE Ultrasonics Symposium, San Juan, Puerto Rico, Oct 2000

Modeling of the Ultrasonic/Sonic Driller/Corer: USDC

S. Sherrit, X. Bao, Z. Chang, B.P. Dolgin, Y. Bar-Cohen
Jet Propulsion Laboratory, California Institute of Technology, Pasadena, CA
D. Pal, J. Kroh, T. Peterson
Cybersonics Inc., Erie, PA

Abstract –Future NASA missions to Mars require sampling techniques for in-situ analysis and/or sample return to Earth. One of the major limitations of sample collection on Mars and other low gravity environments using conventional drilling is the need for high axial force during drilling. In order to address this problem an ultrasonic/sonic drilling/coring (USDC) mechanism based on an ultrasonic horn driven by a piezoelectric stack has been developed. The horn drives a free mass, which resonates, between the horn and drill stem. Tests have shown that this device addresses some of the key challenges to this NASA objective of planetary in-situ analysis or sampling. The USDC is lightweight (450 g), requires low preload (< 5N) and can be driven at low power (5W). The device has been shown to drill various rocks including granite, diorite, basalt and limestone. Although the drill is driven electrically at 20 kHz, a substantial sub-harmonic acoustic component is found that is crucial to drilling performance. Models that explain this low frequency coupling in the horn, free mass, drill stem and rock will be presented.

I. INTRODUCTION

A schematic of the ultrasonic/sonic driller/corer (USDC) is shown in Figure 1 along with a photograph of the device attached to a test rig in the test rig. The device consists of three main parts; an ultrasonic actuator, a free mass and a drill stem. Circuit analysis of the actuator based on the equivalent circuit of a piezoelectric and acoustic elements as discussed by Mason[1],[2] was reported on previously[3]. The horn was found to have a resonance at 21.5 kHz and the free tip velocity at resonance was determined to be linear with respect to the applied voltage and ranged from 1 to 10 m/s depending on the acoustic load.

The vibrations of the horn tip excite the free mass, which resonates between the horn tip and the top of the drill stem at frequency of the order of 1000 Hz. Acoustic energy in the free mass resonator is transferred to the top of the drill stem and propagates to the bit/rock interface where the rock is excited past its ultimate strain and fractures. In order to determine the critical issues related to the control and optimization of the drill initial modeling of the acoustic interaction at the various interfaces of the drill are presented.

The three interfaces studied are: 1) the interaction of the horn tip with the free mass, 2) the interaction of the free mass with the drill stem and 3) the interaction of the base of the drill stem (bit) with the rock.

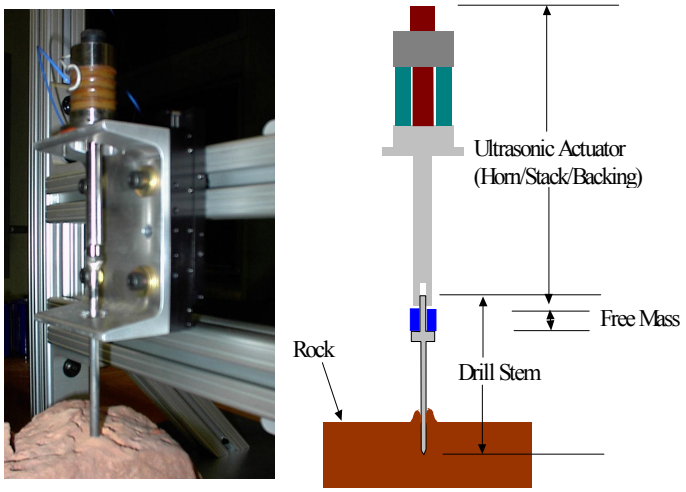

Figure 1. Photograph and Schematic of the Ultrasonic/Sonic Driller/Corer

Finally issues related to the integration of the various interface models will be discussed.

II. MODELING

In order to proceed with the modeling the velocity/ displacement of the horn tip during operation is required. Since the velocity/displacement depends on the acoustic load a reasonable estimate of the velocity range can determined by calculating the horn tip velocity for the case where it is free and when the acoustic impedance is perfectly matched to produce maximum power in the acoustic load. The velocity of the tip as a function of the applied peak AC voltage is shown in Figure 2 for the two cases. The reasons for using the case where the acoustic load is ideal rather than clamped are twofold. Firstly the acoustic power transferred to the rock is substantial which means that horn is well matched to the rest of the acoustic elements and secondly in order for the device to operate efficiently a gap must be present which means that for a substantial portion of the time the tip is not in contact with the free mass. For a peak AC voltage of 200 Volts on the drill the velocity is found to range between 1.25 m/s for the ideal load and 13.6 m/s for the free tip. The modeling of the interaction of the free mass can now be

determined since the range of speeds of the horn tip have been set.

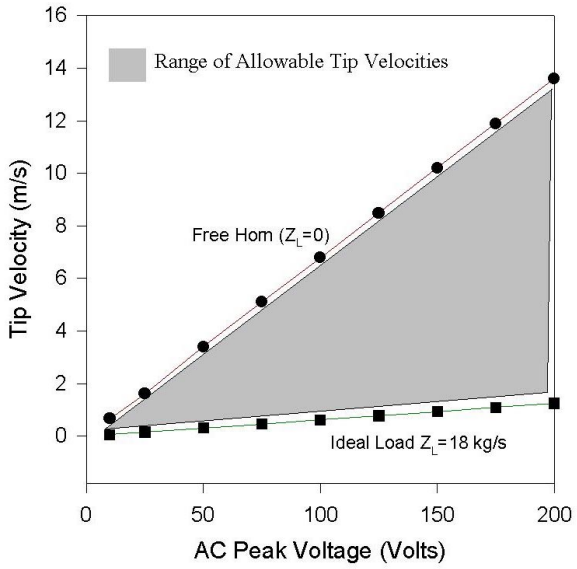

Figure 2. The range of speed for the horn tip for an ideal load and for the unloaded horn.

1) 1) Horn Tip – Free Mass Interaction

The free mass is driven by the horn tip, which vibrates at resonance frequency. A schematic of the model is shown in Figure 3. The tip displacement is harmonic and is describe by

$$u = u_0\cos(\omega t + \theta). \quad (1)$$

The velocity of the horn tip is found by taking the time derivative of the displacement and is

$$v = -\omega u_0 \sin(\omega t + \theta) = v_t \sin(\omega t + \theta). \quad (2)$$

Assuming the energy loss and time duration of the impact is negligible and the mass of the horn is much larger than

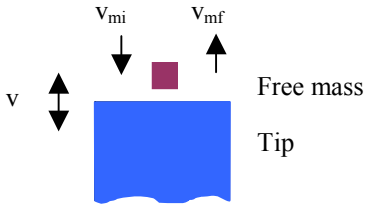

Figure 3. A schematic of the free mass horn tip interaction model.

the free mass, we find using conservation of momentum and energy that

$$v_{mf} = v_{mi} + 2v \quad (3)$$

where v_{mi} is the free-mass velocity prior to interaction with horn and v_{mf} is the free mass velocity after interaction with the horn. A computer simulation model, which traces the positions of the free mass until it leaves the tip vibration range ($2u_0$) was written. The routine calculates the free mass speed after interaction with the horn. By tracking the free mass velocity the routine allowed us to explore this driving mechanism as a function of the initial phase (θ in Eq.1) of tip vibration. At t=0 the free mass crosses the plane of full extension of the tip (u_0). The speed of the free mass as it leaves the interaction region versus the initial phase is shown in Figure 4 for various ratios of v_{mi}/v_t , where v_t is peak tip velocity.

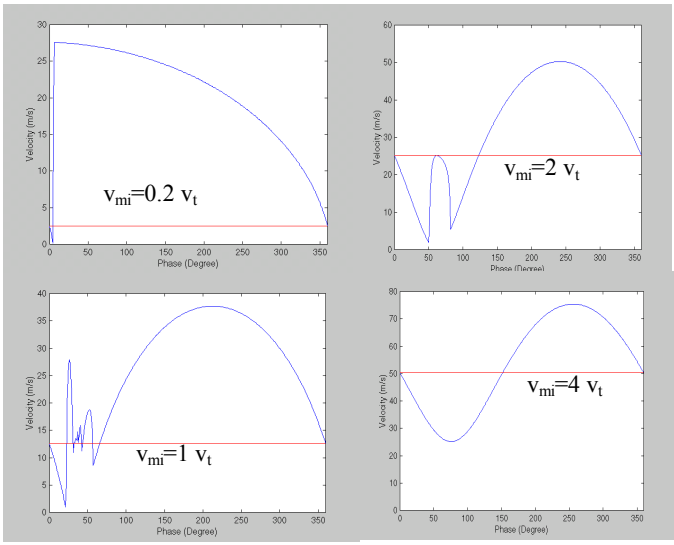

Figure 4. The free mass velocity after interaction with the horn for v_{mi}=0.2, 1, 2, 4v_t for v_t = 12.5 m/s

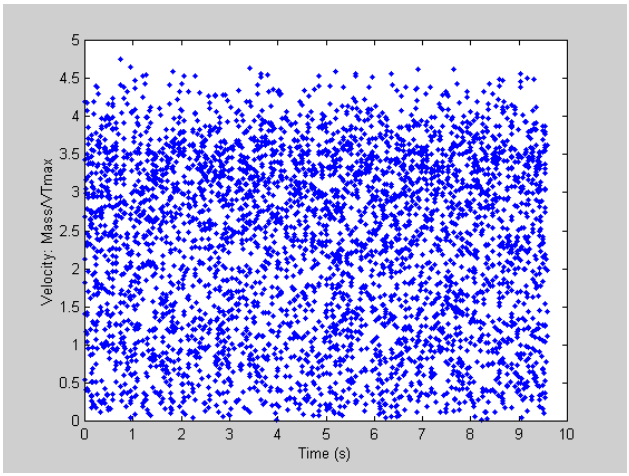

Figure 5. The free mass velocity/maximum tip velocity as a function of time.

For all cases there is a net increase in the free mass velocity after interaction with the horn when averaged over phase. Impact studies using FE modeling are currently being investigated to determine the effective mass of the horn tip and the validity of using the large mass approximation. The computer model, based on collision theory, also traces the movements of the free mass and the horn when the free mass

is driven between the horn and the drill bit. The movement of the horn is due to the reaction force on the horn tip and the force of gravity. In the calculation the mass of the free mass is set to 1 gram, the tip velocity amplitude is set to 1.26 m/s corresponding to displacement amplitude of 10 μm. The horn mass was 800 g. The energy loss of the free mass in each round trip is set at 75%. The simulation results shown in Figure 5 represent the ratio of the free mass velocity to the maximum horn tip velocity as a function of time Figure 6 shows the horn tip position as a function of time.

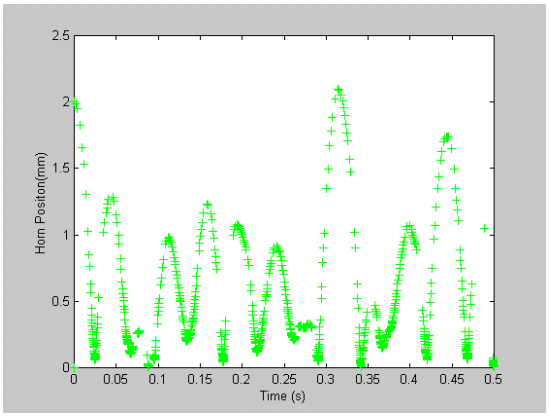

Figure 6. The horn position as a function of time determined from model

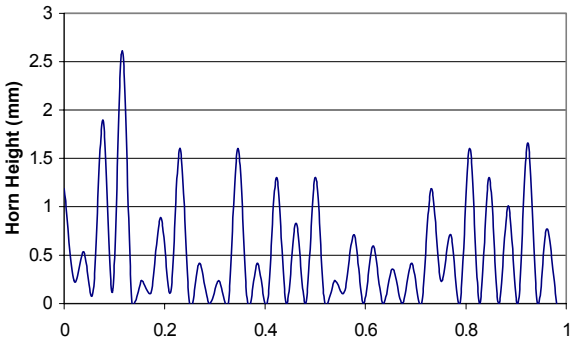

Figure 7. The horn position as a function of time determined from high-speed camera.

The size, frequency and randomness of the jumps are confirmed by experimental observations shown in Figure 7 of the horn tip determined using a high-speed camera.

2) Free mass, Drill stem Interaction

The free mass impacts the top of the drill stem and creates a stress wave that propagates to the bit end. A finite element model was utilized to investigate the impact and resultant stress wave. Figure 8 shows results for the case where a cylindrical steel stem/bit of diameter 3.0 mm and length 100 mm with a concentric top cap of diameter 12 mm and length 6 mm. The impact used in the model is that of a free mass of 2 g with speed 1 m/s. The free mass has a curved surface at the contact area with a curvature of 10 mm. The free mass is assumed to be rigid and the bit end of the drill stem is clamped. Figure 8 shows the displacement of the surface of the free mass and the top surface of the drill stem during impact as a function of time. Figure 9 shows the resultant stress wave as a function of time at the bit end of the drill stem.

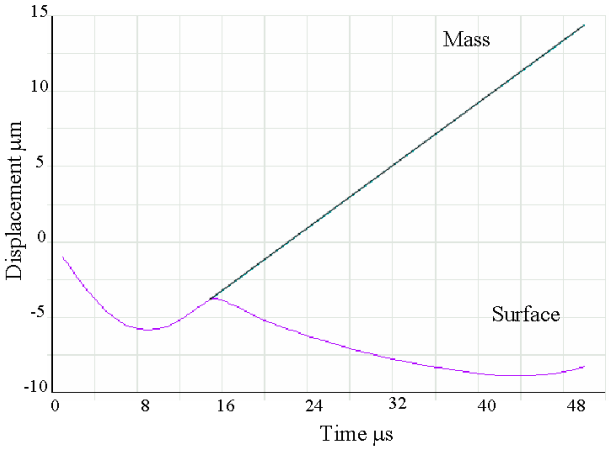

Figure 8. The displacement as a function of time of the free mass and the top surface of the drill stem after impact.

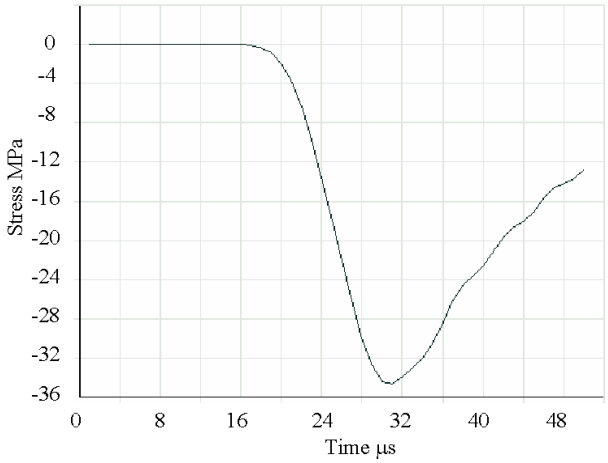

Figure 9. The stress as a function of time for the free mass at the bottom surface of the drill stem after impact.

3) Bit Rock Interaction

In order to better understand the fracture of rocks under impact loading from a drill or a corer, a finite element model was developed using ANSYS. For the purpose of simplifying the problem, the rock is modeled as a circular cylinder with bottom surface fixed and the drill/corer impacts at the center of the top surface. This simplification makes the problem axis-symmetric. By using the axis-symmetric elements available in ANSYS, the original three-dimensional problem is now reduced to a two-dimensions. The element size is made very fine near the drill/corer bit, and becomes coarser and coarser as it goes further away from the bit.

Figure 10 shows a typical mesh for the problem outlined above (Diameter = 20 cm., depth = 10 cm.).

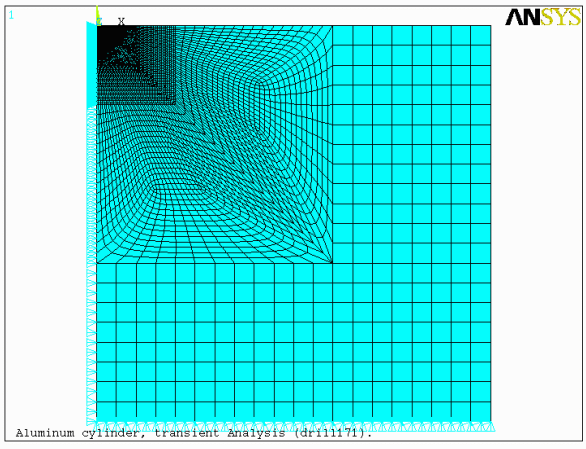

Figure 10. The mesh used to solve the bit rock interaction

Preliminary results were derived by assuming that the circular cylinder is made of isotropic material with a Young's modulus of 9.9 GPa and poisons ratio of 0.3. The impact loading from the drill is estimated for a 2 gram mass traveling at 3 m/s to be 3 time the stress shown in Figure 9. with a duration of 40 µsec. The stress pulse was applied to the top of a 15-cm long drill stem (not shown in Figure 10).

Contour maps of the maximum principal strain were plotted and used as indication of fracture of rocks. Figures 11 show the contour maps for the cylinder for drilling and coring, respectively. The drill bit is 3 mm in diameter. The corer has an inner diameter of 2 mm and an outer diameter of 3 mm.

These results show qualitative features of the rock fracture under ultrasonic/sonic drilling or coring. Figure 11 shows that the highest principal strain occurs at the edge of the drill bit and that the highest principal strain appears at both the outer and inner edge of the corer. This implies that the fracture is likely at the edge, which is confirmed by viewing the high speed filming during drilling. Upon comparing the various strain profiles in Figure 11, we find that the maximum principal strain under the coring is higher than that beneath the drill, and the area of high principal strain under coring is larger than that under drilling. This implies that with the same outer diameter and under the same loading, a corer will drill faster than a solid drill of the same diameter. This effect has been observed during experiments. The results have shown how drilling and coring can be achieved with little or no preload. The next challenge is to integrate each of the models in order to determine the limits and optimization of the USDC.

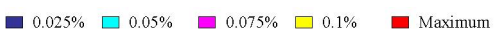

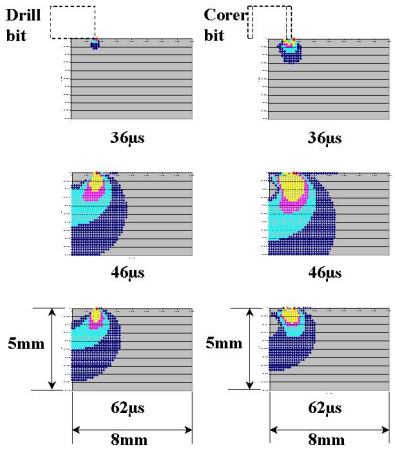

Figure 11. The principle strain profile at various times after impact of the free mass on the drill stem for a drilling bit and a coring bit (OD = 3.0mm).

IV. Conclusions

Models that explain the low frequency coupling of the USDC and the drilling under low axial preload have been presented which in general correlate well with experimental studies. The results suggest a variety of avenues for optimization of the device. Current efforts are underway to integrate the various models to allow for the determination of a system model that would allow for control.

V. Acknowledgment

The authors would like to thank J.D. Carson for design and fabrication of the test apparatus. The research at the Jet Propulsion Laboratory (JPL), a division of the California Institute of Technology, was carried out under the Mars and Deep Space Exploration Programs, while, a JPL SBIR Phase II program funded work at Cybersonics Inc.

References

[1] W.P. Mason, Electromechanical Transducers and Wave Filters, Princeton, NJ, Van Nostrand, 1948

[2] W.P. Mason, Physical Acoustics and the Properties of Solids, D. Van Nostrand Co., Princeton, NJ, 1958

[3]S. Sherrit, B.P. Dolgin, Y. Bar-Cohen, D. Pal, J. Kroh, T. Peterson "Modeling of Horns for Sonic/Ultrasonic Applications," Proceedings of the IEEE International Ultrasonics Symposium, Lake Tahoe, CA, October 1999, pp. 647-651